Title: Binding under conflict conditions: state-space analysis of multivariate EEG synchronization.
Authors: Knyazeva MG, Carmeli C, Fornari E, Meuli R, Small M, Frackowiak RS, Maeder P
Journal: Journal of cognitive neuroscience
Year: 2011 Sep
Volume: 23
Issue: 9
Pages: 2363-75
DOI: 10.1162/jocn.2010.21588

Binding under Conflict Conditions: State–Space Analysis of Multivariate EEG Synchronization

Maria G. Knyazeva[1], Cristian Carmeli[2], Eleonora Fornari[1,3], Reto Meuli[1], Michael Small[2], Richard S. Frackowiak[1,4], and Philippe Maeder[1]

Abstract

■ Real-world objects are often endowed with features that violate Gestalt principles. In our experiment, we examined the neural correlates of binding under conflict conditions in terms of the binding-by-synchronization hypothesis. We presented an ambiguous stimulus ("diamond illusion") to 12 observers. The display consisted of four oblique gratings drifting within circular apertures. Its interpretation fluctuates between *bound* ("diamond") and *unbound* (component gratings) percepts. To model a situation in which Gestalt-driven analysis contradicts the perceptually explicit bound interpretation, we modified the original diamond (OD) stimulus by speeding up one grating. Using OD and modified diamond (MD) stimuli, we managed to dissociate the neural correlates of Gestalt-related (OD vs. MD) and perception-related (bound vs. unbound) factors. Their interaction was expected to reveal the neural networks synchronized specifically in the conflict situation. The synchronization topography of EEG was analyzed with the multivariate S-estimator technique. We found that good Gestalt (OD vs. MD) was associated with a higher posterior synchronization in the beta-gamma band. The effect of perception manifested itself as reciprocal modulations over the posterior and anterior regions (theta/beta-gamma bands). Specifically, higher posterior and lower anterior synchronization supported the bound percept, and the opposite was true for the unbound percept. The interaction showed that binding under challenging perceptual conditions is sustained by enhanced parietal synchronization. We argue that this distributed pattern of synchronization relates to the processes of multistage integration ranging from early grouping operations in the visual areas to maintaining representations in the frontal networks of sensory memory. ■

INTRODUCTION

In the natural environment, objects often have features that violate Gestalt principles according to which perceptual input is organized into groups. Yet the brain "effortlessly" solves the so-called binding problem—that is, it segregates elements in complex scenes and integrates features that belong to the same object. To explore binding under challenging conditions, we chose the paradigm of bistable perception, where, in the absence of a "correct" Gestalt solution, the monitoring and the updating of sensory information lead to dramatic fluctuations of stimulus interpretation (Zeki, 2004; Leopold & Logothetis, 1999). Similarly striking perceptual regroupings can happen under ordinary viewing conditions, for example, as a result of a weak sensory input (Summerfield, Tobias, Mangels, & Hirsch, 2006). Thus, iterative binding is at the heart of unstable perception. Apart from its volatility, binding seems to occur in the same way for stimuli open to single or multiple interpretations (Zeki, 2004; Kovacs, Papathomas, Yang, & Feher, 1996). Moreover, the stability of visual input across various interpretations allows one to dissociate stimulus- from perception-related processes, making ambiguous visual displays an attractive model for studying the neural correlates of the brain machinery of integration.

According to the binding-by-synchronization (BBS) hypothesis, the integration of representations of features processed by distributed neuronal assemblies is coded by their synchronization (Uhlhaas et al., 2009; Engel, Fries, & Singer, 2001; Gray, 1999; Singer, 1999). Thus, the level of cooperation in involved networks should dissociate bound and unbound percepts. This idea has been exemplified by studies focused on *long-distance bivariate synchronization* (Melloni et al., 2007; Knyazeva, Fornari, Meuli, Innocenti, & Maeder, 2006; Knyazeva, Fornari, Meuli, & Maeder, 2006; Rose, Sommer, & Buchel, 2006; Varela, Lachaux, Rodriguez, & Martinerie, 2001; Rodriguez et al., 1999). However, a great many visual binding operations occur within and between spatially and functionally clustered cortical areas (Shipp, Adams, Moutoussis, & Zeki, 2009; Bartels & Zeki, 1998, 2006; Singer, 2004). Therefore, one would expect to find distributed *clusters of synchronized activity*.

[1]Centre Hospitalier Universitaire Vaudois (CHUV) and University of Lausanne, Lausanne, Switzerland, [2]Hong Kong Polytechnic University, Hung Hom, Kowloon, Hong Kong, [3]CIBM (Centre d'Imagerie Biomédicale), Lausanne, Switzerland, [4]IRCCS Santa Lucia, Roma, Italy

To reveal such a landscape of inter-area synchronization related to binding, we applied the method of whole-head mapping by a multivariate S-estimator (Carmeli, Knyazeva, Innocenti, & De Feo, 2005) to high-resolution EEG. The S-estimator is a technique derived from dynamical systems theory that measures synchronization by relating it to the shrinking of the embedding dimension of a network of neural oscillators underlying different electrode sites. Recently, the method was successfully used to analyze synchronization topography in normal and pathological brains (Knyazeva et al., 2010; Jalili et al., 2007; Carmeli et al., 2005). To model a situation in which early stimulus-driven analysis contradicts a perceptually explicit interpretation, we presented an ambiguous stimulus, the "diamond illusion." This consists of four oblique gratings drifting within circular apertures. The interpretation of such a display fluctuates between *bound* (diamond) and *unbound* (individual gratings) percepts.

To make a bound interpretation of the stimulus more difficult, we changed the original display by speeding up one of the four component gratings (Figure 1 and Supplementary movies). In relation to a possible interhemispheric asymmetry of binding (Hellige, 1996), we used two modified stimuli, with the left and the right distinct gratings, respectively. The resulting set of stimuli allowed us to dissociate the neural correlates of stimulus-related (original display vs. modified display) and perception-related (bound vs. unbound) processes. We tested the idea that a bound interpretation of the modified stimuli would require additional involvement of frontal-parietal networks. In the frame of a factorial design, the related synchronized clusters were expected to be unveiled in a stimulus by perception interaction.

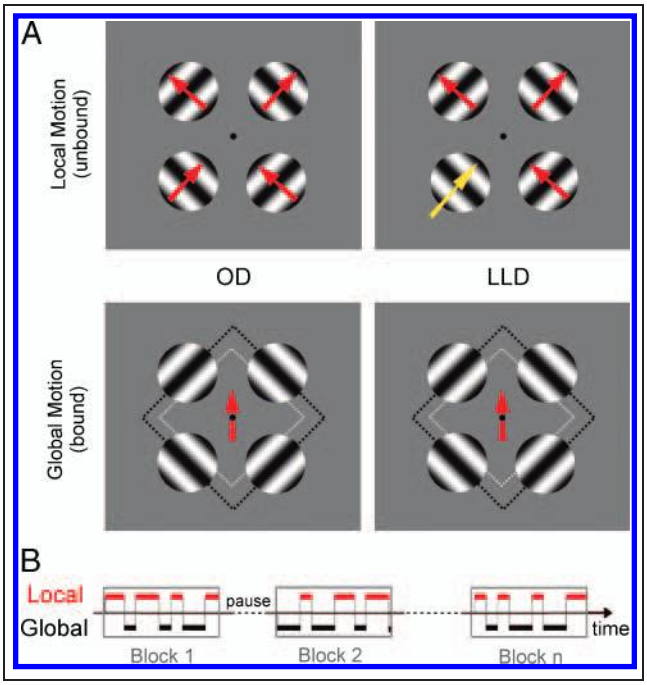

Figure 1. Schematic diagrams of diamond stimuli and EEG sessions. (A) The original stimulus (upper left image) consisted of four oblique gratings drifting within circular apertures (for a detailed description, see the Methods section). The LLD stimulus (upper right image) had its lower left grating (designated by the enlarged yellow arrow) accelerated. The LRD stimulus contained the lower right grating modified (not shown). As shown by the arrows, all the stimuli can be perceived as local motion (top row) or global motion (bottom row). (B) An example of the start of an EEG session is shown. Each subject viewed the OD, the LLD, and the LRD stimuli presented in 60-sec observation periods (blocks) designated here as gray boxes. The tracking of local (unbound) and global (bound) motion percepts by an observer is shown as an alternation between upper (red, global motion) and lower (black, local motion) levels within an observation period. For details, see the Methods section.

METHODS

Subjects

Sixteen adults without known neurological or psychiatric illness and with normal or corrected-to-normal vision were selected for EEG recording (after two preliminary practice sessions) from volunteers recruited mostly among the students of the University of Lausanne and of the Federal Polytechnic School of Lausanne. All subjects gave written informed consent. All procedures were approved by the local Ethics committee of Lausanne University and conformed to the Declaration of Helsinki (1964) of the World Medical Association concerning human experimentation. Because of excessive artifacts or an insufficient number of epochs in one or more conditions, the EEGs of four subjects were removed from analysis. Data from the remaining 12 right-handed participants (7 women and 5 men; mean age = 25.4 years, *SD* = 7.6 years) are presented here. All subjects were paid for their participation in EEG recording sessions.

Stimuli and Protocol

We used an ambiguous stimulus called the "diamond illusion" (Alais, Blake, & Lee, 1998). It consists of four oblique gratings drifting within circular apertures (Figure 1A, Supplementary movies). The interpretation of such a display fluctuates between local patterns (individual gratings) and a global coherent object ("diamond"). Seen locally, the gratings appear to move orthogonally to their orientation, whereas perceived globally, all four gratings appear to drift upward as if they were parts of a single occluded "diamond." In addition to the original diamond (OD) stimulus, we used two modified diamond (MD) stimuli, in which the lower left (LLD) or the lower right (LRD) grating drifted at double speed. Therefore, in total, we applied three stimuli (OD, LLD, and LRD), which resulted in six perceptual conditions (global and local percepts of each stimulus).

The display comprised 0.5 cpd sinusoidal luminance gratings drifting at 45° or 135° with a speed of 2 Hz through circular apertures of 4° in diameter. The apertures formed a virtual square with a center-to-center separation of 6°. The drifting speed in a modified aperture of the MD stimuli

was 4 Hz. All the gratings had a Michelson contrast of 70%. A fixation point in the center of the display subtended a 0.4° visual angle. The observers viewed stimuli, displayed with E-prime stimulation software (Psychology Software Tools, Inc., Pittsburgh, PA), on a PC monitor with a refresh rate of 75 Hz from a distance of 57 cm. The stimuli were presented in 60-sec observation periods (blocks) in an order randomized across subjects (Figure 1B). A uniform gray screen of same space-averaged luminance as the stimuli (32 cd/m^2) was displayed between the stimulation blocks.

During the initial practice session, naive observers were presented with the OD stimulus and instructed to maintain the fixation point and to report their percepts verbally. Those who clearly perceived alternating global and local motion in the perceptual episodes of several seconds were selected for the next training session. In the second session, all the stimuli (OD, LLD, and LRD) were presented. The observers were asked to track the duration of the local and global motion percepts by pressing one of two buttons of a response pad but to ignore the periods of perceptual uncertainty or incomplete percepts (e.g., two upper gratings bound). Subjects who reported the least frequently observed percept (usually the global interpretation of the LRD stimulus) during the time sufficient for the EEG analysis were invited for the third (EEG) session. During an EEG session, each subject saw all the stimuli, with four to six blocks per stimulus. Their responses with the right or left pointer finger (counterbalanced across subjects) were recorded synchronously with EEG by an acquisition computer. They were analyzed off-line and used as the basis for EEG segmentation.

Control of Eye Movements

In a separate session, we monitored four subjects with an eye tracking system (SensoMotoric Instruments GmbH, Teltow, Germany). We used the built-in 9-point routine for the calibration of subjects' point of gaze. The eye movement data and the experimental condition were time locked by triggering the eye tracking system through a serial connection with the E-prime software. The eye positions were sampled at 50 Hz and stored on a PC for off-line analysis, which we performed with Matlab (MathWorks, Natick, MA). We removed from the analysis time intervals during which the gaze position could not be determined, that is, the readings for 0.25 sec before and 0.5 sec after the start of a blink. We assessed the stability of fixation through the percentage of time in which the point-of-gaze was within a circle (Ø 3°) centered on a fixation point. All subjects showed permanent fixation spanning 91% to 96% of the recording time across all conditions.

EEG Recording and Preprocessing

The EEG data were collected in a semidark room with a low level of environmental noise while each subject viewed the stimuli. To control the quality of recordings, the EEG tracings were constantly monitored on-line. We used the 128-channel Geodesic Sensor Net (EGI, Eugene, OR). All the electrode impedances were kept less than 30 kΩ; the recommended limit for the high-input-impedance EGI amplifiers is 50 kΩ (Ferree, Luu, Russell, & Tucker, 2001). The recordings of vertex reference EEG were made using a 12-bit analog-to-digital converter, a digitization rate of 1000 samples per second, and a low-pass filter set to 100 Hz. They were further filtered (FIR, band-pass filter of 1–70 Hz, notch at 50 Hz), segmented into nonoverlapping 1-sec epochs using NS 4.2 software (EGI), rereferenced against the common average reference (CAR), and transformed into the Laplacian by computing a two-dimensional surface Laplacian via EEGLAB software (Delorme & Makeig, 2004).

Artifacts in all channels were edited off-line: first, automatically, on the basis of an absolute voltage threshold (100 μV) and on a transition threshold (50 μV) and then on the basis of a thorough visual inspection. The sensors that recorded artifactual EEG (>20% of the recording time) were corrected using the bad channel replacement tool (NS 4.2; EGI). The number of artifact-free epochs entered into the analysis for each of the six conditions was on average 73 ± 26 ranging from 61 ± 19 epochs related to the local percept of the OD stimulus to 85 ± 27 epochs related to the local percept of the LLD stimulus. To avoid transitional processes, we discarded the first and the last seconds of each perceptual interval between two consecutive reversals.

Finally, the data were filtered into four EEG frequency bands: theta (3–7 Hz), alpha (7–13 Hz), beta (13–30 Hz), and gamma (30–48 Hz). To this end, we used digital filtering with no phase shift via a constrained least squares FIR filter (Selesnick, Lang, & Burrus, 1996) implemented by the Matlab function FIRCLS.

S-estimator as a Measure of Synchronization

The S-estimator exploits a theoretical consequence of synchronization phenomena to indirectly quantify the synchronization within a set of measurements of arbitrary cardinality (Carmeli et al., 2005). Considering a network of dynamical systems, the observable dimensionality (embedding dimension) of the whole dynamical network decreases as a consequence of interactions among the network elements (Boccaletti, Valladares, Kurths, Maza, & Mancini, 2000; Brown & Kocarev, 2000).

The S-estimator indirectly estimates the synchronization-induced contraction of the embedding dimension by measuring the dispersion (entropy) of the eigenvalues of the correlation matrix of a multivariate set of measurements.

Formally, given a P-variate time series $\mathbf{Y}$, the S-estimator is defined as

$$S = 1 + \frac{\sum_{i=1}^{P} \lambda'_i \log(\lambda'_i)}{\log(P)} = 1 - \frac{E(\lambda')}{\log(P)}$$

where $\lambda_i' = \lambda_i/P$ designates the normalized eigenvalues of the correlation matrix of the multivariate time series **Y**, and $E(\lambda')$ is their entropy.

The entropy $E(\lambda')$ accounts for how many dimensions are significantly visited by the observed trajectory. When all the normalized eigenvalues are roughly of the same value (maximal dispersion of eigenvalues), all the state–space dimensions are almost equally visited; in this case, $E(\lambda')$ is maximal [close to $\log(P)$], consequently S is close to 0, meaning no contraction of the embedding dimension—that is, no synchronization. Alternatively, when nearly all the normalized eigenvalues are roughly 0 and a few of them are appreciably nonzero (minimal dispersion), only few state–space dimensions are visited; in this case, $E(\lambda')$ is minimal (close to 0), consequently S is close to 1, meaning maximal contraction of the embedding dimension—that is, complete synchronization.

Thus, the S-estimator is a multivariate linear measure that fits modern high-density EEG setups by allowing a reconstruction of the whole-head surface topography of synchronization. Compared with the widely used indices of phase locking, the S-estimator does not require an extraction of phase, which is an advantage for broadband phase-ambiguous signals like EEG (Boashash, 1992). Although the S-estimator is not sensitive to nonlinear correlations among signals, such an approach seems to be appropriate for normal EEGs that are usually found to be linear (Andrzejak et al., 2001).

The S-estimator was calculated from the EEGs preprocessed into epochs. The S-estimator is a measure of synchronization in the time domain, so we applied it to filtered EEG time series with spectral content in each of the four frequency bands of interest (see the EEG recording and preprocessing section). To assess the whole-head synchronization topography, we computed the S-estimator sensor-wise over the cluster of locations defined by the sensor itself and the surrounding ones belonging to its second-order neighborhood (Carmeli et al., 2005). A typical cluster spanned, on average, a region of approximately 12 cm in diameter. Although the evaluation of long-distance synchronization is possible with the S-estimator, such an analysis was not needed to answer the questions posed in this study.

The interpretation of surface EEG measures of synchronization is limited because of their contamination by volume conduction and reference electrode effects (Nunez et al., 1997). These unwanted effects can be minimized with a high-resolution Laplacian, which isolates the source activity under each sensor (Srinivasan, Winter, Ding, & Nunez, 2007). According to the simulations by these authors, all effects of volume conduction are removed from a Laplacian estimated from dense electrode arrays (≥128 sensors) at distances greater than approximately 3 cm. Yet along with volume conduction, a Laplacian removes genuine synchronization of widely distributed source regions, which can be captured by CAR EEG. In our recent studies, we demonstrated that interhemispheric synchronization estimated with CAR EEG signals reliably correlates with the fMRI activation of neural assemblies presumably involved in synchronized activity (Knyazeva, Fornari, Meuli, Innocenti, et al., 2006; Knyazeva, Fornari, Meuli, & Maeder, 2006). Here we examined the topography of multivariate synchronization on the basis of a combination of the Laplacian and CAR EEG, thus encompassing both small and intermediate spatial scales of EEG dynamics. All the computations were performed within the Matlab environment (http://aperest.epfl.ch/docs/software.htm).

Supplementary Analysis of EEG Energy

Although all reasonable precautions to reduce the effects of volume conduction were taken, there still remains the possibility that the reported effects on synchronization topography could be a side effect of differences in signal-to-noise ratio rather than being related to effective synchronization. To figure out whether such a possibility could be the case, we performed a supplementary analysis of EEG energy. This analysis was especially important for CAR EEG.

The CAR applied to high-density EEG serves as a spatial filter that filters out low spatial frequencies, including deep sources. Therefore, CAR EEG reflects predominantly the activity of shallow dipole layers located in gyral crowns (Srinivasan et al., 2007). The interpretation of such EEG first suffers from local changes in power, which can affect synchronization measurements through volume conduction. Therefore, a comparison between the changes in power and those in synchronization is a useful strategy for clarifying the interpretation of synchronization measurements. In the case of associated changes, one would suspect that surface synchronization simply follows local power changes.

We computed the power spectra with the multitaper method (Mitra & Pesaran, 1999). This method involves the multiplication of data segments with multiple tapers before Fourier transformation and effectively concentrates spectral estimates across a specified frequency band. We used a set of tapers to achieve a spectral concentration greater than ±3 Hz. Eventually, the average power in the frequency band of interest was computed via the integral of the power spectral density for each subject, sensor, and condition. On the basis of these values, whole-head energy maps were constructed. To minimize the effects of volume conduction on the synchronization results, we removed sensors with significant energy changes from the S-estimator ANOVA maps (Figures 3–5).

Moreover, to take into account even nonsignificant changes in power, we computed the Pearson correlation coefficients between changes in EEG synchronization and energy. The statistical procedure was analogous to the one used for the correlation analysis with behavioral indices. Overall, a few sensors showed significant correlations at $p < .05$. Such sensors were also removed from the S-estimator ANOVA maps (Figures 3–5).

Correlation Analysis

To assess to what extent synchronization topography is related to behavioral observables within a perceptual state, we investigated the correlation topography between synchronization and the mean durations of the intervals between two consecutive switches separately for each perceptual interpretation of each stimulus. The correlation maps were computed by estimating the Pearson correlation coefficient sensor-wise. To determine whether the correlation values were significantly nonzero, we applied a nonparametric statistical approach—a permutation-based test (Higgins, 2004). The permutations were constrained as for the ANOVA (see the Statistical inference section). The p values obtained after performing 5000 permutations were corrected for multiple comparisons by means of the BH false discovery rate method. Finally, correlations were considered significant at sensors with corrected p values lower than .05.

Statistical Inference

Statistical assessment was performed using the linear model—repeated measures ANOVA—in the context of sequentially occurring perceptual alternations. Specifically, we used a 2 × 3 factorial design including the Perception factor (two levels: global and local) and the Stimulus factor (three levels: OD, LLD, and LRD). Statistical inference was performed independently for each frequency band of interest. Synchronization and power/energy estimates that entered into the statistical analysis were computed for each subject by using a summary statistic (the mean) over values obtained for all epochs belonging to the same condition.

Considering that synchronization and power/energy values vary over a finite interval and thus cannot have a Gaussian distribution, we applied a nonparametric permutation approach. This approach, which requires only minimal assumptions for validity, provides a flexible and intuitive methodology for the statistical analysis of data from neuroimaging experiments (Nichols & Holmes, 2002).

However, the permutation procedure has to be refined according to a repeated measure design. Indeed, repeated measurements of the same subject's responses will be correlated and cannot be regarded as interchangeable, and interchangeability is a requirement for using permutation procedures. Formally, a set of labels on the data is interchangeable if the distribution of the statistic to be evaluated is the same as the labeling. In our study, the subjects can be regarded as labels on the values of synchronization or energy (i.e., the data), and the statistic to be evaluated is the ANOVA F statistic. Therefore, we constrained the permutations so as to limit each subject's contribution to one observation at each level of the permuted within-subject factor (Suckling & Bullmore, 2004).

A p value for each sensor was obtained by performing 5000 permutations, which were identical for each sensor to retain the spatial covariance structure of the data. To get a statistical significance for the whole map, these p values had to be corrected for multiple comparisons. As the computation of each S-estimator value involved its neighbors, the p values were corrected by means of the BH false discovery rate method (Benjamini & Hochberg, 1995). The BH-corrected p values were verified to be at least $p < .05$.

We also measured the sizes of the effects. To this end, we computed the *partial omega squared*, which is defined as a proportion of variance of the dependent variable that is explained by the factor or contrast of interest. The values of the partial omega squared vary between 0 and 1. According to Cohen (1988), a value of this measure close to .01 represents a small effect size, .06 a medium effect size, and .15 a large effect size. To follow a conservative statistical approach and to highlight the most pronounced effects, we report the maps thresholded at 0.06 (medium effect size).

RESULTS

Behavioral Data

In common with other bistable stimuli, the normalized durations (expressed as a fraction of the mean percept duration) of perceptual episodes induced by OD and MD stimuli followed a gamma distribution (Figures 2A and S1). The coherence index, which is defined as the proportion of the total observation period during which global motion is perceived, was significantly ($p < .05$, Wilcoxon matched-pairs signed-ranks test) different for the OD versus both MD stimuli (Figure 2B). Thus, compared with the OD stimulus, the competition between the two perceptual interpretations induced by the MD stimuli was biased in favor of the unbound percept. It is noteworthy that this happened because of the longer durations of the local perception episodes compared with the unchanged durations of the global perception episodes (Figure 2C). In particular, the group mean values for local percept durations were 3.9, 4.9, and 6.6 sec for OD, LLD, and LRD, respectively. The mean global percept durations were 4.7 sec (OD), 4.8 sec (LLD), and 5.2 sec (LRD). The difference between the local mean values was significant for the OD versus the LLD ($p < .05$) and for the OD versus the LRD ($p < .01$). The difference between the MD stimuli was significant at a level of $p = .1$. Presumably, this is a very conservative estimate because several subjects were discarded because of their overwhelmingly local perception of the LRD stimulus.

Topography of Multivariate Synchronization

The main effect of stimulus in CAR EEG (Figure 3, top row) was significant for a cluster of occipital and parietal sensors across the beta-gamma bands. At the theta-beta frequencies,[1] it was supplemented by a right hemisphere

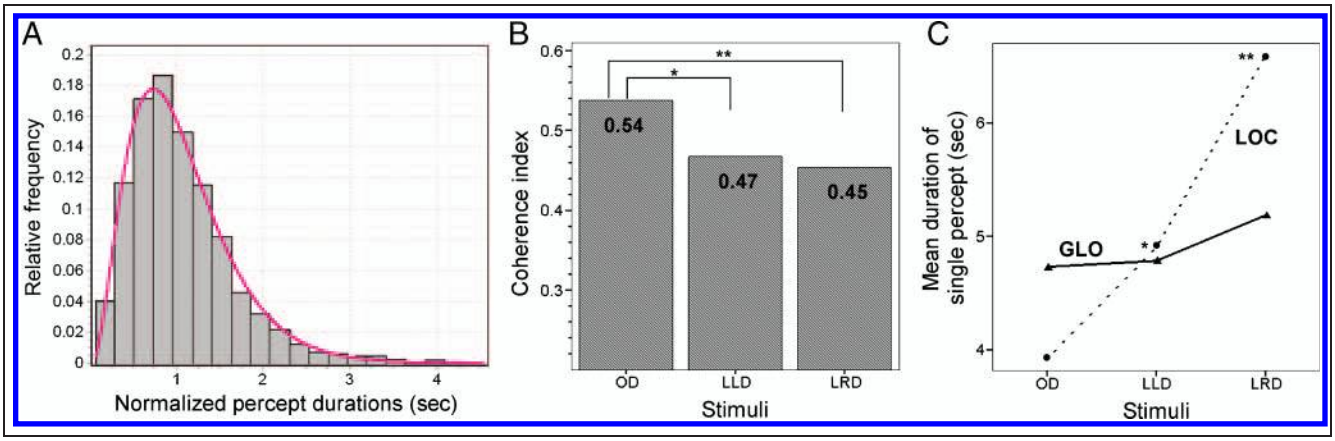

Figure 2. Behavioral data. (A) The gamma distribution of the normalized durations of perceptual episodes summarized for all the diamond stimuli. The fitted gamma distribution has shape (k) and scale (λ) parameters of 3.22 and 2.85, respectively. The fitting was significant at $p < .02$ (Kolmogorov–Smirnov test). (B) Coherence index—the proportion of total observation period during which global motion was perceived—is shown for the OD, LLD, and LRD stimuli. Significant differences between the stimuli in coherence index are designated by $*p < .05$ or $**p < .01$. (C) Mean durations of the global (GLO, solid line and triangles) and local (LOC, dotted line and circles) perception episodes for the same stimuli. Significant differences in the duration of perceptual episodes between OD and MD were found only for the local perceptual episodes and are designated as in panel B.

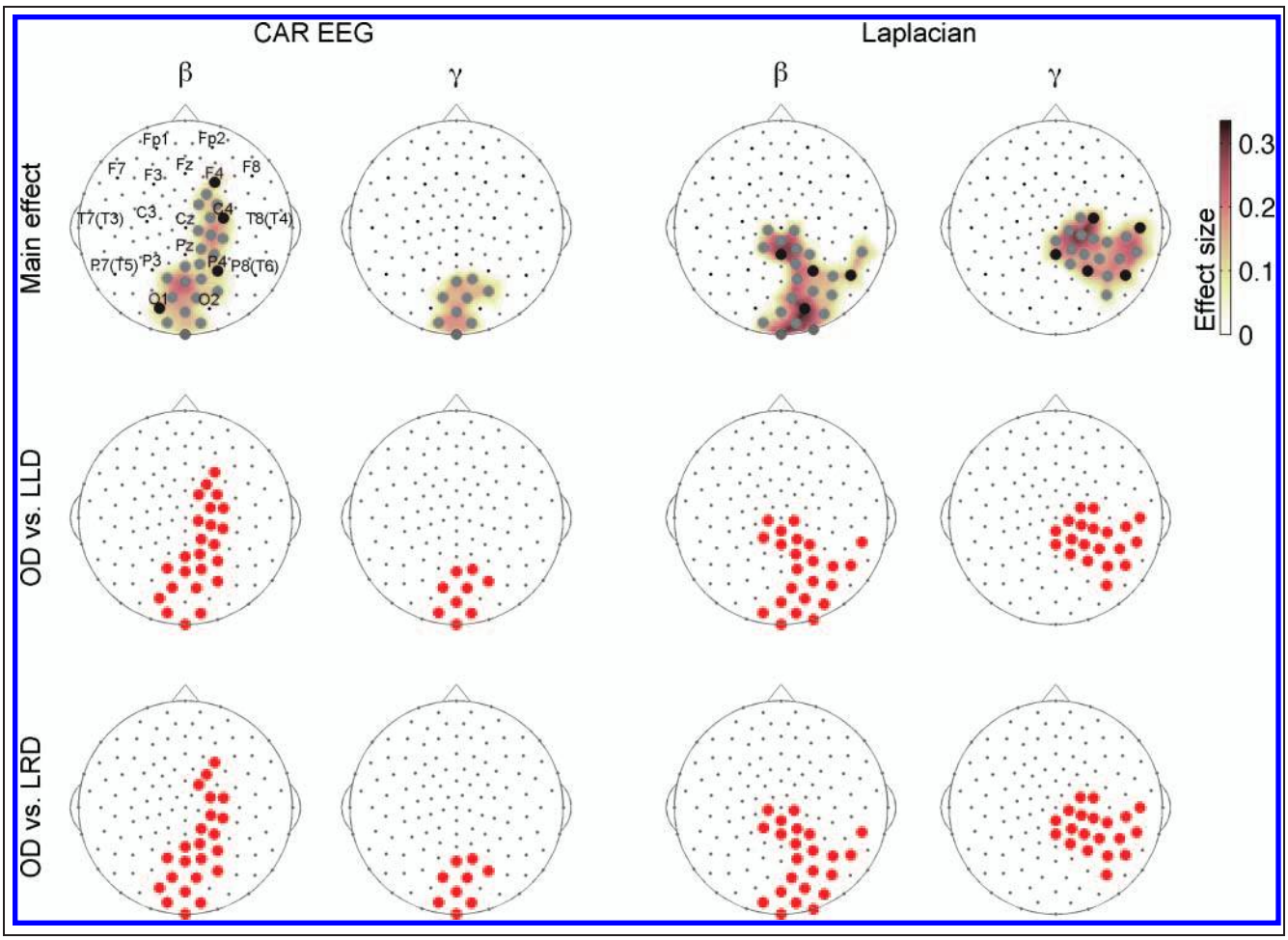

Figure 3. Gestalt-driven changes in multivariate EEG synchronization. The whole-head maps for the S-estimator show the surface topography of the main stimulus effect (top row) and of the planned contrasts OD versus LLD (middle row) and OD versus LRD (bottom row). The S-maps are presented in the beta and gamma frequency bands for CAR EEG (first and second columns) and the Laplacian (third and fourth columns). They are superimposed on the diagrams of the Geodesic 128-channel Sensor Net. The sensors corresponding to the International 10–20 System are shown with black circles. They are labeled in the upper left diagram. The large circles (irrespective of color) designate significant effect. All the effects are shown at $p < .05$, BH corrected and thresholded at .06 (partial omega squared according to Cohen, 1988). In the S-maps for planned contrasts, red sensors correspond to OD > MD. In the S-maps for the main effect, the colored surface (obtained by a trilinear interpolation from the three nearest electrodes) represents partial omega squared.

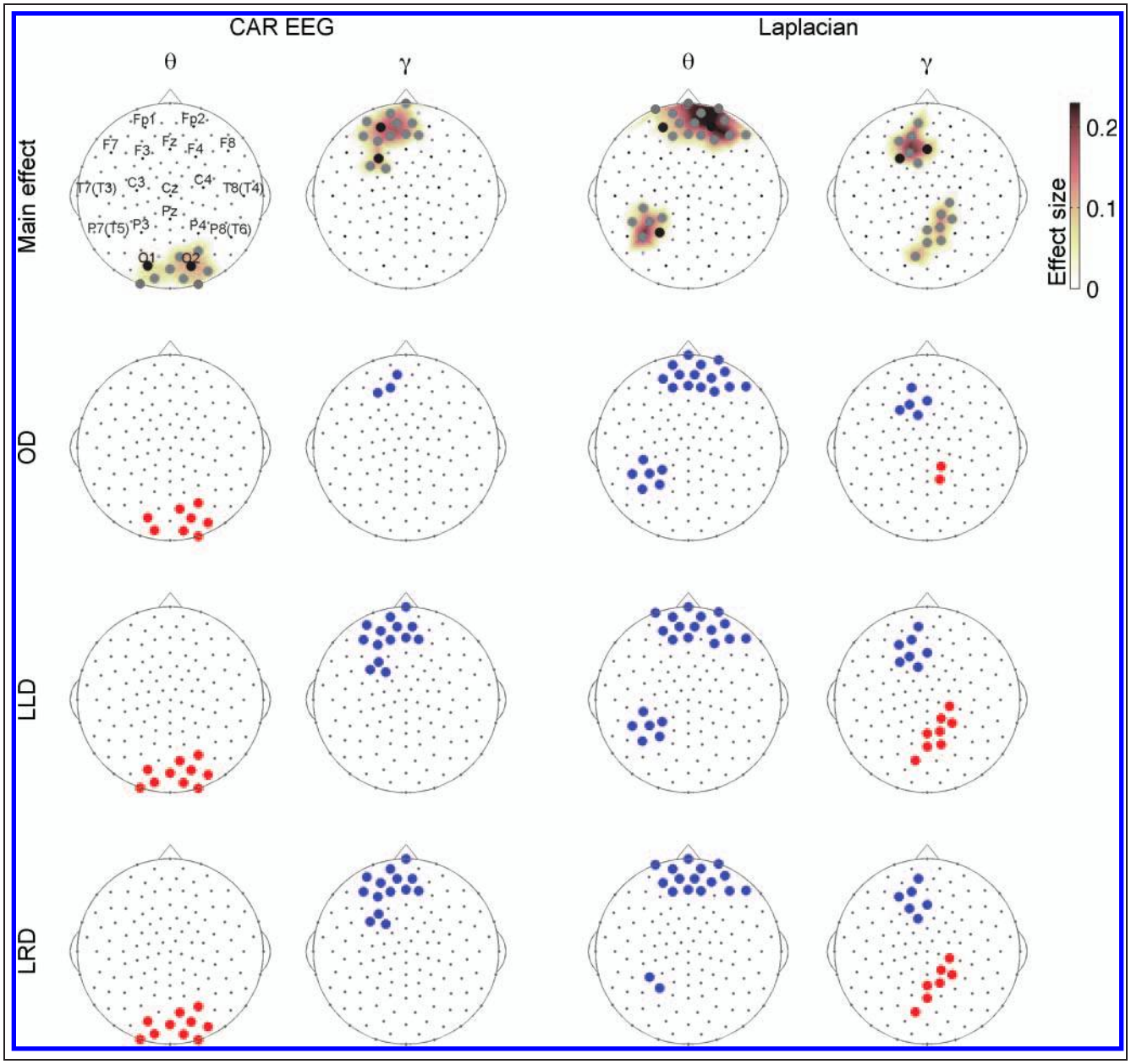

Figure 4. Perception-related changes in multivariate EEG synchronization. The whole-head difference maps for S-estimator show the surface topography of the main perception effect (top row) and the planned contrasts between bound and unbound (global motion vs. local motion) percept for the OD (second row), LLD (third row), and LRD (bottom row) stimuli, supporting the main effect in the beta and gamma frequency bands of CAR EEG (on the left) and the Laplacian (on the right). In the S-maps for planned contrasts, red sensors correspond to global > local, whereas blue sensors correspond to global < local. Other designations are as in Figure 3.

cluster extending dorsally between parietal and mid-frontal locations. The analysis of the Laplacian revealed that the main effect of the stimulus is significant for occipital and parietal sensors (theta-beta bands) and for temporal and parietal ones (beta-gamma bands) over the right hemisphere. The planned contrasts (OD vs. LLD and OD vs. LRD) revealed higher synchronization in response to the original stimulus for both CAR EEG and the Laplacian. The strongest effects both in terms of effect size and in terms of the number of sensors involved were observed in the beta-gamma bands. The closest agreement in the topography between CAR EEG and the Laplacian was found in the beta band.

The supplementary analysis showed a few sensors with significant but relatively weak stimulus effects on EEG energy (Figure S2). In the gamma band, the locations of energy and S-estimator changes were different (cf. Figures 3 and S2). In the beta band, these topographies also differed, apart from a small left occipital cluster common to both EEG parameters. However, there were no correlations between the changes in S-estimator and energy.

The main effect of Perception is shown in Figure 4. For CAR EEG, the largest clusters involved are located over the occipital (theta band) and left frontal regions (beta-gamma bands). A remarkable feature of the global-to-local

contrasts is that each perceptual interpretation of the stimuli is supported by opposite changes in intraregional synchronization over the frontal and occipital regions. In particular, global perception is accompanied by an increase of the S-estimator in the occipital theta cluster but a decrease in the frontal alpha and gamma clusters. Vice versa, for local perception, the decrease in occipital synchronization occurs in parallel with an increase in frontal synchronization.

In the Laplacian, the main effect of Perception was expressed in the frontal (theta and gamma bands), left temporo-parietal (theta), and right parieto-occipital (gamma) clusters (Figure 4). The global interpretation of the diamond stimuli was accompanied by desynchronization in frontal clusters (as in CAR EEG) and in the left temporo-parietal cluster. The right parieto-occipital cluster demonstrated behavior similar to that of the occipital cluster in CAR EEG: An increase in synchronization was related to the global interpretation and its decrease associated with the local interpretation of the stimuli, the changes being opposite to the frontal ones. The global-to-local contrasts showed that this effect was much more extensive for the MD stimuli than for the OD stimulus.

A supplementary analysis of EEG energy showed no effects in the beta-gamma band and significant but weak changes over the left parieto-temporal region in the theta band (Figure S3). The latter did not overlap with any S-estimator effects (cf. Figures 4 and S3).

The interaction between stimulus and perception was significant for the midline parieto-occipital cluster of sensors in CAR EEG (Figure 5). Because our focus here was on the EEG correlates of a bound percept that depended on stimulus properties, we examined only those contrasts that captured such effects, that is, those between stimuli producing a bound percept and between bound and unbound percepts for different stimuli. The latter contrasts turned out to be significant for the midline parieto-occipital cluster in the beta band. In response to the LRD stimulus, the S-estimator increased during global perception. However, it increased during local perception in response to the other two stimuli—LLD and OD (Figure 5). There was no significant stimulus by perception interaction in EEG energy.

In addition to gathering these categorical data separating alternative perceptual interpretations, we performed a correlation analysis, which allowed us to look at the relationship between EEG synchronization and behavior within each perceptual state. We found significant inverse correlations consistent across all the stimuli in the gamma band between the duration of a global percept and the frontal synchronization for CAR EEG and direct correlations between the duration of a global percept and the synchronization in the parietal cluster in the beta band for the Laplacian (Figure 6). These correlations show that the lower the prefrontal synchronization and the higher the parietal synchronization, the longer the duration of a bound percept. By contrast, the duration of local perception did not correlate with regional synchronization.

DISCUSSION

By applying multivariate mapping of synchronization to high-resolution EEG, we have demonstrated for the first time the whole-head landscape of synchronized clusters related to multistage visual integration. Specifically, the stimulus-driven grouping appears to be related to higher posterior EEG synchronization. This effect was largely

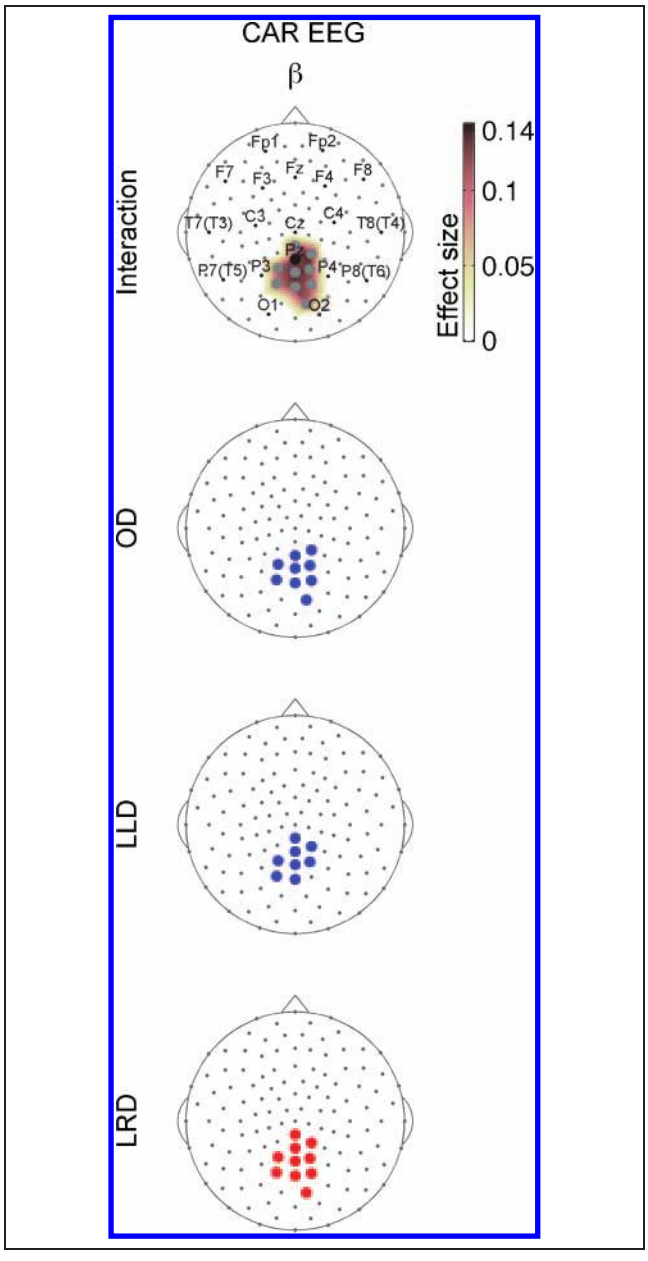

Figure 5. Interaction between stimulus and perception effects. The topography of interaction (top diagram) and the planned contrasts between bound and unbound percepts for the OD, LLD, and LRD stimuli are shown for CAR EEG. Other designations are as in Figures 3 and 4.

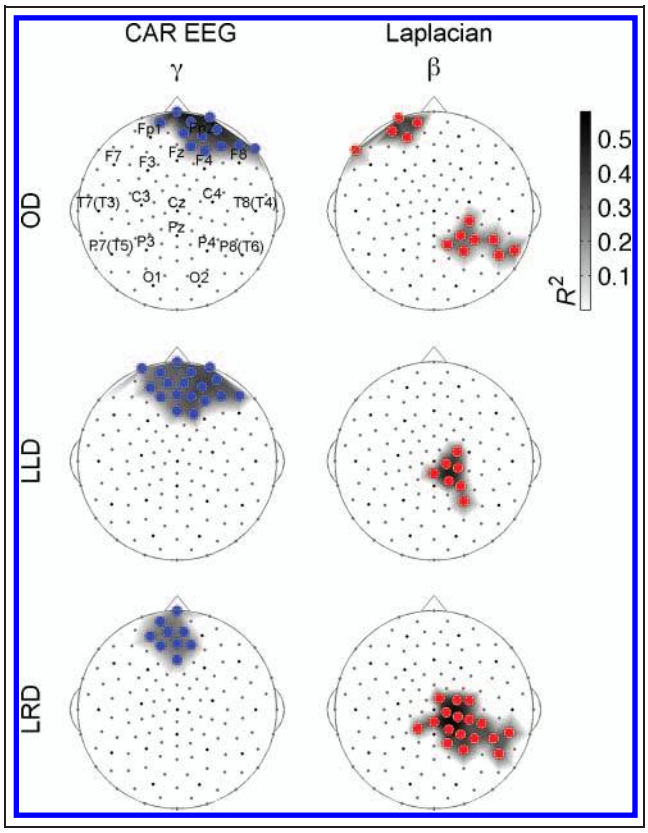

Figure 6. Surface topography of correlations between S-estimator and mean duration of episodes of global perception. Significant Pearson correlations at $p < .05$ (BH-corrected) are shown for OD, LLD, and LRD stimuli in the gamma frequency band of CAR EEG and beta frequency band for the Laplacian. The sensors with direct correlations are designated by red circles, with inverse correlations—by blue circles. The size of the correlations is reported as the coefficient of determination (R^2) defined as the square of the Pearson correlation value.

expressed at beta-gamma EEG frequencies. The fluctuations of perception were related to the reciprocal modulations of synchronization over occipito-parietal and prefrontal regions. Specifically, higher posterior and lower anterior S-estimator values supported the bound percept and vice versa—lower posterior and higher prefrontal synchronization accompanied the unbound percept. These changes encompassed both fast EEG frequencies (the beta-gamma band) and slow EEG frequencies (the theta band). Under challenging perceptual conditions, when the results of early stage grouping contradicted a perceptually explicit global interpretation, the latter was additionally supported by increased high-frequency synchronization over the parietal region. Importantly, as confirmed by the supplementary analysis, these effects were associated with interarea synchronization at a centimeter scale rather than with local changes of EEG energy. As predicted by the BBS hypothesis, the majority of the synchronization effects observed here were limited to the beta-gamma EEG frequencies. Yet the occipital and prefrontal synchronization fluctuated with perceptually explicit interpretations in the theta band.

Stimulus-driven Synchronization

In the primate brain, motion appears to be processed in a hierarchical manner, suggesting that visual areas play differential roles in perception. According to current models, motion processing consists of several stages, in which an initial short-range (local) analysis and a subsequent long-range integration are implemented (Berzhanskaya, Grossberg, & Mingolla, 2007; Snowden, Treue, Erickson, & Andersen, 1991; Mather, Cavanagh, & Anstis, 1985; Adelson & Movshon, 1982). Because the neural representations of the components of a diamond stimulus are separated anatomically within and between the cerebral hemispheres, we expected the integration machinery would be dissociable from that underlying local processing on the basis of interareal synchronization. If the BBS hypothesis holds true, we expected that posterior synchronization clusters would be sensitive to stimulus properties.

Indeed, EEG synchronization in the beta-gamma frequencies increased in response to the original stimulus (compared with the response to modified stimuli). The topography of this effect, that was reproducible across EEG methods, was limited to the occipito-parietal regions. Considering that the Laplacian estimate sources are located close to the head surface while CAR EEG captures deeper or more spread-out sources, the significant effects detected with both types of EEG indicate that the diamond stimulus induces widespread synchronization among both shallow and deep sources.

Such an interpretation is in line with our previous studies, where we have shown that interhemispheric synchronization in CAR EEG may be associated with activations of the dorsal and ventral stream areas (Knyazeva, Fornari, Meuli, Innocenti, et al., 2006; Knyazeva, Fornari, Meuli, & Maeder, 2006). In particular, bilateral iso-oriented gratings compared with orthogonally oriented gratings synchronized CAR EEG across hemispheres and increased the BOLD signal bilaterally in the lingual/fusiform gyrus and in the parieto-occipital fissure, territories implicated in grouping and object recognition. Importantly, interhemispheric EEG coherence correlated with fMRI activation in both sites.

Therefore, stimulus-dependent motion integration takes place at multiple nodes of the processing system and seems to be a temporally extended process that includes both early and later processing stages. Similarly distributed networks are involved in the grouping of other visual attributes (for a review, see Palmer, Brooks, & Nelson, 2003).

Synchronization Dynamics Underlying Perceptual Interpretation of Stimulus

We have found that the synchronization clusters distributed over the occipital, parietal, and prefrontal regions are sensitive to the perceptual interpretation of stimuli. On a coarse scale, this topography corresponds to the regions activated during maintenance of a bound percept as

shown in neuroimaging studies (Fang, Kersten, & Murray, 2008; Seymour, Karnath, & Himmelbach, 2008; Fink et al., 1997; for a review, see Sasaki, 2007). Specifically, the effect of perception manifested itself as reciprocal modulations of synchronization over the occipito-parietal and prefrontal regions. In so doing, the global percept was supported by higher posterior and lower anterior synchronization compared with the local percept. The interpretation of posterior synchronization in terms of the BBS hypothesis is quite straightforward and consistent with conclusions from other human studies (Melloni et al., 2007; Knyazeva, Fornari, Meuli, Innocenti, et al., 2006; Knyazeva, Fornari, Meuli, & Maeder, 2006; Rose et al., 2006; Varela et al., 2001; Rodriguez et al., 1999). The posterior clusters of synchronized sensors shown with the Laplacian indicate that perceptual binding is not limited to the occipital visual areas but extends to the parietal cortex. This is consistent with the clinical observations that damage of the parietal cortex results in binding failure (Humphreys, Hodsoll, & Riddoch, 2009; Friedman-Hill, Robertson, & Treisman, 1995) as well as being consistent with fMRI accounts of feature binding (Shafritz, Gore, & Marois, 2002).

In animal models, the effects of ambiguous *plaid stimuli* are of particular interest for this discussion. Such stimuli consist of two superimposed gratings moving in different directions. They may be perceived as a single plaid pattern (bound percept) or as two component gratings (unbound percept). With only slight changes of the stimuli, perception can be biased in favor of pattern or component motion. In cats, neurons distributed in the visual areas synchronize their discharges when responding to pattern motion, but not when responding to component motion (Castelo-Branco, Goebel, Neuenschwander, & Singer, 2000). However, in contrast to the large-scale human synchronization studies, not all animal experiments support the BBS hypothesis (Dong, Mihalas, Qiu, von der Heydt, & Niebur, 2008; Croner & Albright, 1999; Shadlen & Movshon, 1999). This discrepancy can be explained by the fact that, unlike spiking, EEG time series are mainly composed of synchronized activity, which results in a complicated relationship between the two types of activity dependent on a variety of factors (Goense & Logothetis, 2008). This also means that synchronization dynamics can be more easily demonstrated within large-scale neuronal populations. Indeed, in monkeys, synchrony in spiking activity showed no regular changes in bound versus unbound condition, whereas gamma band synchrony in field potentials was significantly stronger in the bound condition (Palanca & DeAngelis, 2005).

The prefrontal desynchronization associated with a bound percept was an unexpected finding and yet was well replicated across stimuli and EEG methods. Together with the dynamics of posterior synchronization, it created a "see-saw" effect: an increase of posterior synchronization associated with an anterior desynchronization for global and vice versa for local percepts. The explanation of a prefrontal decrease in synchronization associated with the bound percept is not that obvious and calls for a more detailed discussion. In contrast with occipital synchronization, the frontal and parietal S-estimator values correlate with the duration of ongoing global perceptual episodes (Figure 6); that is, cooperation in these networks somehow affects the stabilization of a current representation. Stabilization effects have been previously seen in experiments on intermittent bistable perception (Keizer, Colzato, & Hommel, 2008; Pastukhov & Braun, 2008). They were explained by the involvement of sensory memory, which retains the last percept during a blank period, thus leading to its stabilization in the ensuing rivalry (Pearson & Brascamp, 2008). Such a stabilization correlates with the activation of the prefrontal and parietal cortices during a blank period (Sterzer & Rees, 2008). We suggest that the fronto-parietal mechanisms that sustain the representation of an ongoing stimulus in our experiment and those that support its retention (i.e., that are reactivated during a blank period) are based on these same networks.

The direction of changes in prefrontal synchronization between bound and unbound percepts is consistent with the involvement of memory networks in our continuous perceptual task. Indeed, we have found that maintaining a bound representation of a stimulus requires lower synchronization than do its unbound (parallel) representations (Figure 4). Because the pFC deals with integrated representations of objects, we expected the information maintained during global perception to be packed into a single chunk whereas during local perception into four chunks. Consequently, the maintenance of four items would involve more distributed neural networks than maintaining one item. A comparable phenomenon has been observed recently in a neuroimaging study that contrasted the bound representation of "what" and "where" information with separate representations of object and spatial information (Sala & Courtney, 2007). The integrated representation activated a smaller area relative to unimodal representations. Although in agreement with our results, this interpretation requires more direct experimental testing before it can be accepted with confidence.

Binding under Challenging Conditions

To model a challenging perceptual situation, we modified the original display so as to make early stage stimulus-based representations contradict *global interpretation* of a stimulus. Indeed, bistable perception of the MD stimuli appeared to be biased in favor of their *local interpretation*. With that, an intervention in the *right* visual field affected perception more than the same intervention in the *left* visual field. Considering that the subjects removed from our analysis because of an insufficient number of EEG epochs lacked the epochs for the global perception of the LRD stimulus, the lateralization of this effect in the general population may be stronger than the tendency shown here.

The greater right-visual-field effect of a speeded-up grating can be related to left hemisphere superiority in

time-based analysis (Rutherford, 2003; Nicholls, 1994; Efron, 1963) and/or to the right hemisphere advantage in global versus local processing (Hellige, 1996) and grouping operations (Gazzaniga, 2000; Stiles & Nass, 1991). Such an interpretation is consistent with the predominantly right hemisphere synchronization that supports a good Gestalt (Figure 3) and a global interpretation of all stimuli (Figure 6).

The global perception of the most challenging LRD stimulus was accompanied by additional parietal synchronization (Figure 5). Also, the global percept of both MD stimuli was accompanied by increased synchronization in the beta (CAR EEG) and gamma (the Laplacian) bands over parietal regions (Figure 4). Because the Laplacian isolates activity under each electrode, the effects in the Laplacian presumably reflect synchronization between sources located close to the head surface in the superior parietal lobule.

This region is well known for operating in situations when additional processing is required to come up with a decision. Thus, it is more engaged when observers are not confident about their interpretations. Such examples include low confidence recognition judgments, memory, or perceptual decisions (Fleck, Daselaar, Dobbins, & Cabeza, 2006; Moritz, Glascher, Sommer, Buchel, & Braus, 2006; Varela et al., 2001; Dolan et al., 1997; for a review, see Ciaramelli, Grady, & Moscovitch, 2008). This region is also involved in conflict resolution. For instance, subjects instructed to determine the form from motion within a randomly moving dot field, while ignoring either direction of motion or stimulus location, activate the superior parietal lobule (Wittfoth, Buck, Fahle, & Herrmann, 2006). Recently, an association between the parietal beta activity and the detection of weak coherent motion signals has been reported (Donner et al., 2007).

In the preceding examples, the superior parietal lobule implements operations related to attention, learning, and/or integration with higher order information. However, in our experiment, the subjects' attention was controlled by the requirement that they had to report on stimulus motion in both perceptual conditions. On the other hand, our instructions did not provide any bias in favor of one interpretation that could have provoked implicit learning. Therefore, the synchronization dynamics over the parietal region seem to indicate the presence of basic built-in machinery that supports weak alternative interpretations being tested by the brain. This machinery could be part of a previously proposed mechanism that implements a permanent search for and testing of perceptual hypotheses, especially active under challenging conditions (Leopold & Logothetis, 1999).

Acknowledgments

This work was supported by the Swiss National Science Foundation grant no. 3100A0-103993/1 and by the Hong Kong University Grants Council (UGC) Competitive Earmarked Research Grant (CERG) no. PolyU5269/06E. The authors thank Ms. D. Polzik for assistance in the preparation of the manuscript. M. G. K. and C. C. contributed equally to this work.

Reprint requests should be sent to Maria G. Knyazeva, Department of Clinical Neuroscience, CHUV, 1011 Lausanne, Switzerland, or via e-mail: Maria.Knyazeva@chuv.ch.

Note

1. Here and further, all the significant effects are described in the text. However, if an effect encompasses more than one EEG frequency band, only bands with the most salient effects are shown in the respective figure.

REFERENCES

Adelson, E. H., & Movshon, J. A. (1982). Phenomenal coherence of moving visual patterns. *Nature, 300,* 523–525.

Alais, D., Blake, R., & Lee, S. H. (1998). Visual features that vary together over time group together over space. *Nature Neuroscience, 1,* 160–164.

Andrzejak, R. G., Lehnertz, K., Mormann, F., Rieke, C., David, P., & Elger, C. E. (2001). Indications of nonlinear deterministic and finite-dimensional structures in time series of brain electrical activity: Dependence on recording region and brain state. *Physical Review E, 64,* 061907.

Bartels, A., & Zeki, S. (1998). The theory of multistage integration in the visual brain. *Philosophical Transactions of the Royal Society of London, Series B, Biological Sciences, 265,* 2327–2332.

Bartels, A., & Zeki, S. (2006). The temporal order of binding visual attributes. *Vision Research, 46,* 2280–2286.

Benjamini, Y., & Hochberg, Y. (1995). Controlling the false discovery rate—A practical and powerful approach to multiple testing. *Journal of the Royal Statistical Society, Series B, Methodological, 57,* 289–300.

Berzhanskaya, J., Grossberg, S., & Mingolla, E. (2007). Laminar cortical dynamics of visual form and motion interactions during coherent object motion perception. *Spatial Vision, 20,* 337–395.

Boashash, B. (1992). Estimating and interpreting the instantaneous frequency of a signal: I. Fundamentals. *Proceedings of the IEEE, 80,* 520–538.

Boccaletti, S., Valladares, D. L., Kurths, J., Maza, D., & Mancini, H. (2000). Synchronization of chaotic structurally nonequivalent systems. *Physical Review, E, Statistical Physics, Plasmas, Fluids, and Related Interdisciplinary Topics, 61,* 3712–3715.

Brown, R., & Kocarev, L. (2000). A unifying definition of synchronization for dynamical systems. *Chaos, 10,* 344–349.

Carmeli, C., Knyazeva, M. G., Innocenti, G. M., & De Feo, O. (2005). Assessment of EEG synchronization based on state–space analysis. *Neuroimage, 25,* 339–354.

Castelo-Branco, M., Goebel, R., Neuenschwander, S., & Singer, W. (2000). Neural synchrony correlates with surface segregation rules. *Nature, 405,* 685–689.

Ciaramelli, E., Grady, C. L., & Moscovitch, M. (2008). Top–down and bottom–up attention to memory: A hypothesis (atom) on the role of the posterior parietal cortex in memory retrieval. *Neuropsychologia, 46,* 1828–1851.

Cohen, J. (1988). *Statistical power analysis for the behavioral sciences*. New York: Academic Press.

Croner, L. J., & Albright, T. D. (1999). Seeing the big picture: Integration of image cues in the primate visual system. *Neuron, 24,* 777–789.

Delorme, A., & Makeig, S. (2004). EEGLAB: An open source toolbox for analysis of single-trial EEG dynamics including independent component analysis. *Journal of Neuroscience Methods, 134,* 9–21.
Dolan, R. J., Fink, G. R., Rolls, E., Booth, M., Holmes, A., Frackowiak, R. S., et al. (1997). How the brain learns to see objects and faces in an impoverished context. *Nature, 389,* 596–599.
Dong, Y., Mihalas, S., Qiu, F., von der Heydt, R., & Niebur, E. (2008). Synchrony and the binding problem in macaque visual cortex. *Journal of Vision, 8,* 1–16.
Donner, T. H., Siegel, M., Oostenveld, R., Fries, P., Bauer, M., & Engel, A. K. (2007). Population activity in the human dorsal pathway predicts the accuracy of visual motion detection. *Journal of Neurophysiology, 98,* 345–359.
Efron, R. (1963). The effect of handedness on the perception of simultaneity and temporal order. *Brain, 86,* 261–284.
Engel, A. K., Fries, P., & Singer, W. (2001). Dynamic predictions: Oscillations and synchrony in top–down processing. *Nature Reviews Neuroscience, 2,* 704–716.
Fang, F., Kersten, D., & Murray, S. O. (2008). Perceptual grouping and inverse fMRI activity patterns in human visual cortex. *Journal of Vision, 8,* 2.1–2.9.
Ferree, T. C., Luu, P., Russell, G. S., & Tucker, D. M. (2001). Scalp electrode impedance, infection risk, and EEG data quality. *Journal of Clinical Neurophysiology, 112,* 536–544.
Fink, G. R., Halligan, P. W., Marshall, J. C., Frith, C. D., Frackowiak, R. S., & Dolan, R. J. (1997). Neural mechanisms involved in the processing of global and local aspects of hierarchically organized visual stimuli. *Brain, 120,* 1779–1791.
Fleck, M. S., Daselaar, S. M., Dobbins, I. G., & Cabeza, R. (2006). Role of prefrontal and anterior cingulate regions in decision-making processes shared by memory and nonmemory tasks. *Cerebral Cortex, 16,* 1623–1630.
Friedman-Hill, S. R., Robertson, L. C., & Treisman, A. (1995). Parietal contributions to visual feature binding: Evidence from a patient with bilateral lesions. *Science, 269,* 853–855.
Gazzaniga, M. S. (2000). Cerebral specialization and interhemispheric communication: Does the corpus callosum enable the human condition? *Brain, 123,* 1293–1326.
Goense, J. B., & Logothetis, N. K. (2008). Neurophysiology of the bold fMRI signal in awake monkeys. *Current Biology, 18,* 631–640.
Gray, C. M. (1999). The temporal correlation hypothesis of visual feature integration: Still alive and well. *Neuron, 24,* 31–47, 111–125.
Hellige, J. B. (1996). Hemispheric asymmetry for visual information processing. *Acta Neurobiologiae Experimentalis, 56,* 485–497.
Higgins, J. J. (2004). *Introduction to modern nonparametric statistics*. Belmont, CA: Brooks/Cole-Thomson Learning.
Humphreys, G. W., Hodsoll, J., & Riddoch, M. J. (2009). Fractionating the binding process: Neuropsychological evidence from reversed search efficiencies. *Journal of Experimental Psychology: Human Perception and Performance, 35,* 627–647.
Jalili, M., Lavoie, S., Deppen, P., Meuli, R., Do, K. Q., Cuenod, M., et al. (2007). Dysconnection topography in schizophrenia revealed with state–space analysis of EEG. *PLoS One, 2,* e1059.
Keizer, A. W., Colzato, L. S., & Hommel, B. (2008). Integrating faces, houses, motion, and action: Spontaneous binding across ventral and dorsal processing streams. *Acta Psychologica, 127,* 177–185.
Knyazeva, M. G., Fornari, E., Meuli, R., Innocenti, G., & Maeder, P. (2006). Imaging of a synchronous neuronal assembly in the human visual brain. *Neuroimage, 29,* 593–604.
Knyazeva, M. G., Fornari, E., Meuli, R., & Maeder, P. (2006). Interhemispheric integration at different spatial scales: The evidence from EEG coherence and fMRI. *Journal of Neurophysiology, 96,* 259–275.
Knyazeva, M. G., Jalili, M., Brioschi, A., Bourquin, I., Fornari, E., Hasler, M., et al. (2008). Topography of EEG multivariate phase synchronization in early Alzheimer's disease. *Neurobiology of Aging, 31,* 1132–1144.
Kovacs, I., Papathomas, T. V., Yang, M., & Feher, A. (1996). When the brain changes its mind: Interocular grouping during binocular rivalry. *Proceedings of the National Academy of Sciences, U.S.A., 93,* 15508–15511.
Leopold, D. A., & Logothetis, N. K. (1999). Multistable phenomena: Changing views in perception. *Trends in Cognitive Sciences, 3,* 254–264.
Mather, G., Cavanagh, P., & Anstis, S. M. (1985). A moving display which opposes short-range and long-range signals. *Perception, 14,* 163–166.
Melloni, L., Molina, C., Pena, M., Torres, D., Singer, W., & Rodriguez, E. (2007). Synchronization of neural activity across cortical areas correlates with conscious perception. *Journal of Neuroscience, 27,* 2858–2865.
Mitra, P. P., & Pesaran, B. (1999). Analysis of dynamic brain imaging data. *Biophysical Journal, 76,* 691–708.
Moritz, S., Glascher, J., Sommer, T., Buchel, C., & Braus, D. F. (2006). Neural correlates of memory confidence. *Neuroimage, 33,* 1188–1193.
Nicholls, M. E. R. (1994). Hemispheric asymmetries for temporal resolution: A signal detection analysis of threshold and bias. *Quarterly Journal of Experimental Psychology, 47,* 291–310.
Nichols, T. E., & Holmes, A. P. (2002). Nonparametric permutation tests for functional neuroimaging: A primer with examples. *Human Brain Mapping, 15,* 1–25.
Nunez, P., Srinivasan, R., Westdorp, A., Wijesinghe, R., Tucker, D., Silberstein, R., et al. (1997). EEG coherency: I. Statistics, reference electrode, volume conduction, Laplacians, cortical imaging, and interpretation at multiple scales. *Electroencephalography and Clinical Neurophysiology, 103,* 499–515.
Palanca, B. J., & DeAngelis, G. C. (2005). Does neuronal synchrony underlie visual feature grouping? *Neuron, 46,* 333–346.
Palmer, S. E., Brooks, J. L., & Nelson, R. (2003). When does grouping happen? *Acta Psychologica, 114,* 311–330.
Pastukhov, A., & Braun, J. (2008). A short-term memory of multi-stable perception. *Journal of Vision, 8,* 1–14.
Pearson, J., & Brascamp, J. (2008). Sensory memory for ambiguous vision. *Trends in Cognitive Sciences, 12,* 334–341.
Rodriguez, E., George, N., Lachaux, J. P., Martinerie, J., Renault, B., & Varela, F. J. (1999). Perception's shadow: Long-distance synchronization of human brain activity. *Nature, 397,* 430–433.
Rose, M., Sommer, T., & Buchel, C. (2006). Integration of local features to a global percept by neural coupling. *Cerebral Cortex, 16,* 1522–1528.
Rutherford, B. J. (2003). Laterality and pattern persistence in bistable motion perception. *Brain and Cognition, 53,* 335–341.
Sala, J. B., & Courtney, S. M. (2007). Binding of what and where during working memory maintenance. *Cortex, 43,* 5–21.
Sasaki, Y. (2007). Processing local signals into global patterns. *Current Opinion in Neurobiology, 17,* 132–139.

Selesnick, I. W., Lang, M., & Burrus, C. S. (1996). Constrained least square design of FIR filters without specified transition bands. *IEEE Transactions on Signal Processing, 44,* 1879–1892.
Seymour, K., Karnath, H. O., & Himmelbach, M. (2008). Perceptual grouping in the human brain: Common processing of different cues. *NeuroReport, 19,* 1769–1772.
Shadlen, M. N., & Movshon, J. A. (1999). Synchrony unbound: A critical evaluation of the temporal binding hypothesis. *Neuron, 24,* 67–77.
Shafritz, K. M., Gore, J. C., & Marois, R. (2002). The role of the parietal cortex in visual feature binding. *Proceedings of the National Academy of Sciences, U.S.A., 99,* 10917–10922.
Shipp, S., Adams, D. L., Moutoussis, K., & Zeki, S. (2009). Feature binding in the feedback layers of area V2. *Cerebral Cortex, 19,* 2230–2239.
Singer, W. (1999). Neuronal synchrony: A versatile code for the definition of relations? *Neuron, 24,* 49–65, 111–125.
Singer, W. (2004). Synchrony, oscillations, and relational codes. In L. M. Chalupa & J. S. Werner (Eds.), *The visual neurosciences* (Vol. 2, pp. 1665–1681). Cambridge, MA: The MIT Press.
Snowden, R. J., Treue, S., Erickson, R. G., & Andersen, R. A. (1991). The response of area MT and V1 neurons to transparent motion. *Journal of Neuroscience, 11,* 2768–2785.
Srinivasan, R., Winter, W. R., Ding, J., & Nunez, P. L. (2007). EEG and MEG coherence: Measures of functional connectivity at distinct spatial scales of neocortical dynamics. *Journal of Neuroscience Methods, 166,* 41–52.
Sterzer, P., & Rees, G. (2008). A neural basis for percept stabilization in binocular rivalry. *Journal of Cognitive Neuroscience, 20,* 389–399.
Stiles, J., & Nass, R. (1991). Spatial grouping activity in young children with congenital right or left hemisphere brain injury. *Brain and Cognition, 15,* 201–222.
Suckling, J., & Bullmore, E. (2004). Permutation tests for factorially designed neuroimaging experiments. *Human Brain Mapping, 22,* 193–205.
Summerfield, C., Tobias, G., Mangels, G., & Hirsch, J. (2006). Mistaking a house for a face: Neural correlates of misperception in healthy humans. *Cerebral Cortex, 16,* 500–508.
Uhlhaas, P. J., Pipa, G., Lima, B., Melloni, L., Neuenschwander, S., Nikolić, D., et al. (2009). Neural synchrony in cortical networks: History, concept and current status. *Frontiers in Integrative Neuroscience, 3,* 17.
Varela, F., Lachaux, J. P., Rodriguez, E., & Martinerie, J. (2001). The brainweb: Phase synchronization and large-scale integration. *Nature Reviews Neuroscience, 2,* 229–239.
Wittfoth, M., Buck, D., Fahle, M., & Herrmann, M. (2006). Comparison of two Simon tasks: Neuronal correlates of conflict resolution based on coherent motion perception. *Neuroimage, 32,* 921–929.
Zeki, S. (2004). The neurology of ambiguity. *Consciousness and Cognition, 13,* 173–196.

This article has been cited by:

1. Boyd Millar. 2016. Frege's Puzzle for Perception. *Philosophy and Phenomenological Research* **93**:2, 368-392. [CrossRef]
2. Ming Huo, Mieke Heyvaert, Wim Van den Noortgate, Patrick Onghena. 2014. Permutation Tests in the Educational and Behavioral Sciences. *Methodology* **10**:2, 43-59. [CrossRef]
3. Michael X Cohen, Katharina A. Wilmes, Irene van de Vijver. 2011. Cortical electrophysiological network dynamics of feedback learning. *Trends in Cognitive Sciences* **15**:12, 558-566. [CrossRef]